Inorganic Chemistry

pubs.acs.org/IC Article

Photochromic Ln-MOFs: A Platform for Metal-Photoswitch Cooperativity

Corey R. Martin,* Grace C. Thaggard, Ingrid Lehman-Andino, Eduardo Mollinedo, Binod K. Rai, Matthew A. Page, Kathryn Taylor-Pashow, and Natalia B. Shustova

Cite This: *Inorg. Chem.* 2024, 63, 12810−12817 Read Online

ACCESS | Metrics & More | Article Recommendations | Supporting Information

ABSTRACT: Optoelectronic devices based on lanthanide-containing materials are an emergent area of research due to imminent interest in a new generation of diode materials, optical and magnetic sensors, and ratiometric thermometers. Tailoring material properties through the employment of photo- or thermochromic moieties is a powerful approach that requires a deep fundamental understanding of possible cooperativity between lanthanide-based metal centers and integrated switchable units. In this work, we probe this concept through the synthesis, structural analysis, and spectroscopic characterization of novel photochromic lanthanide-based metal−organic materials containing noncoordinatively integrated photoresponsive 4,4′-azopyridine between lanthanide-based metal centers. As a result, a photophysical material response tailored on demand through the incorporation of photochromic compounds within a rigid matrix was investigated. The comprehensive analysis of photoresponsive metal−organic materials includes single-crystal X-ray diffraction and diffuse reflectance spectroscopic studies that provide guiding principles necessary for understanding photochromic unit-lanthanide-based metal−organic framework (MOF) cooperativity. Furthermore, steady-state and time-resolved diffuse reflectance spectroscopic studies revealed a rapid rate of photoresponsive moiety attenuation upon its integration within the rigid matrix of lanthanide-based MOFs in comparison with that in solution, highlighting a unique role and synergy that occurred between stimuli-responsive moieties and the lanthanide-based MOF platform, allowing for tunability and control of material photoisomerization kinetics.

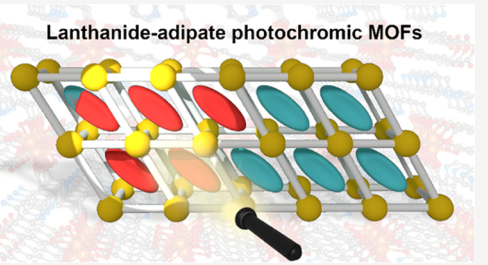

INTRODUCTION

Demands in emerging technologies in the field of optoelectronics attract significant attention toward lanthanide-based materials, and in particular, lanthanide-based metal−organic frameworks (MOFs) due to their applications as diode materials, optical and magnetic sensors, fluorescent probes, and ratiometric thermometers.[1−10] Interest in the area of lanthanide-containing materials is partly driven by the fundamental chemical properties of lanthanides as a class, including the fact that lanthanide-based materials can possess metal centers exhibiting both luminescence and magnetic properties, enabling the design of multifunctional devices (e.g., platforms for biomedical imaging and diagnostics based on magnetic and fluorescent properties).[11−14] Further, the development of materials with intriguing electronic structures and properties can be promoted through the high spin−orbit coupling typically observed for lanthanides.[8,11−14] At the same time, forbidden *f*−*f* transitions give rise to peculiar optical properties such as hypersensitive and narrow emission profiles that can cover a large range of the electromagnetic spectrum (e.g., from 400 to 1600 nm).[8,11−15]

In addition to the mentioned advantages of lanthanides in general, lanthanide-based MOFs (Ln-MOFs) offer the possibility to develop materials with tailorable optical properties through the incorporation of stimuli-responsive molecules either as guests or as a part of the MOF skeleton. In particular, integration of photochromic molecules within Ln-MOFs is a promising approach to probe possible interactions between lanthanide-based metal centers and light-responsive components, which could be used to tune the optical and electronic properties of the bulk material with high spatiotemporal control using light as a noninvasive stimulus.[16−18] In this direction, incorporation of azo compounds in Ln-MOFs is an attractive strategy since photoresponsive azobenzene derivatives integrated in bulk materials have already been applied as, for example, actuators due to significant changes in their molecular conformations, polarity, and light absorption upon their photoisomerization.[19−21] Further, azobenzene derivatives have been used to control liquid crystal domains or photophysical properties of nonlinear optical materials and sensors[22−28] due to their long thermal half-lives, large

Received: March 28, 2024
Revised: May 22, 2024
Accepted: June 11, 2024
Published: June 27, 2024

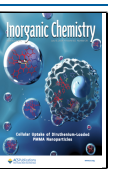

extinction coefficients, high photoisomerization quantum yields, and fatigue resistance.[29−32] While there are several reports on azobenzene inclusion within MOFs, there are very few reports on metal(III)-based photochromic MOFs containing azobenzene (e.g., MIL-101,[33] MIL-53,[34] MIL-68,[34] and MIL-58[35] derivatives), and besides that, the majority of these materials possess photoinactive linkers in combination with d^0 and d^{10} metal centers.[16−18] Further, there are currently no reports in the literature that combine both X-ray diffraction data and photophysical measurements to evaluate how the integration of photochromic azobenzene moieties in Ce-, Nd-, or Pr-MOFs could be leveraged to tailor the photoisomerization behavior of the azobenzene unit. Therefore, a fundamental understanding of how azobenzene derivatives may be employed for tailoring optical and electronic properties of materials containing lanthanide-based metal centers is extremely limited, and the literature reports are scarce.[36−43] In this direction, studies that combine photophysical measurements with X-ray crystallographic analysis of photoswitch-lanthanide interactions are an important first step toward understanding how photochromic molecules can be used to enhance the performance of lanthanide-based materials by offering precise control over the photophysical profile of such metal−organic materials, which defines and broadens the scope of their applications.[44−46] As a result, such studies could lay the foundation for the next generation of optoelectronic devices including logic gates, multilevel anticounterfeiting technologies, and information encryption systems,[47] as well as materials for high-speed data processing.[48]

Herein, we demonstrate synergistic cooperativity between a porous modular scaffold and a noncoordinatively integrated photochromic unit; i.e., we probe how the integration of stimuli-responsive components can affect and direct the photophysics of Ln-based MOFs, and at the same time, how a rigid and modular scaffold can significantly affect the performance of a photochromic moiety for the first time. For that, three novel isoreticular Ln-based MOFs (Ln = Ce, Pr, or Nd) were prepared for the simultaneous integration of 4,4′-azopyridine (Scheme 1). Structural analysis of the prepared series of isostructural lanthanide-based MOFs provides insights into the coordination environment of lanthanide cations within nine-coordinated metal nodes as well as intermolecular interactions between the photochromic moiety and a supramolecular scaffold. To the best of our knowledge, we present the first analysis of the photoisomerization kinetics for azobenzene derivatives integrated within Ce-, Pr-, or Nd-MOFs. The mentioned photoisomerization kinetics of the prepared stimuli-responsive materials was probed using steady-state and time-resolved spectroscopic analysis, demonstrating that an embedded photochromic unit allows for control of the MOF photophysical profile, while at the same time, a rigid matrix defines the photoisomerization rates of a photo-responsive unit. The highlights of these studies showcase lanthanide-based MOFs as a possible platform for harnessing the potential of azo compounds coupled to lanthanide centers for the design of next-generation multifunctional materials, which will include stimuli-responsive sensors, heterogeneous catalysts, and optoelectronics.

Scheme 1. (*Top Left*) Schematic Representation of a Lanthanide-Based Platform Investigated in the Present Work. (*Top Right*) X-ray Crystal Structure of Azo@Ce-MOF. (*Bottom*) The Structures of the Building Units: A Photochromic Azobenzene Derivative, a Nonphotochromic MOF Linker, and a Ln-Based Metal Node[a]

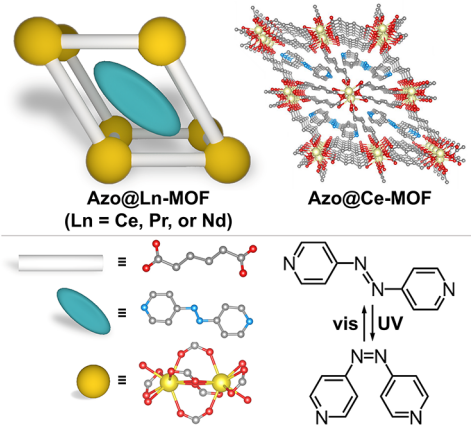

[a]The yellow, gray, red, and blue spheres represent cerium, carbon, oxygen, and nitrogen atoms, respectively. Hydrogen atoms are omitted for clarity.

EXPERIMENTAL SECTION

Materials and General Procedures. Praseodymium(III) chloride hydrate (Sigma-Aldrich, 99.9%), neodymium(III) chloride hexahydrate (Sigma-Aldrich, 99.9%), cerium(III) chloride heptahydrate (Thermo Scientific, 99%), ammonium hydroxide (Thermo Scientific, 28%), 4,4′-azopyridine (Sigma-Aldrich, ≥88%), adipic acid (Sigma-Aldrich, 99%), *N*,*N*-dimethylformamide (DMF, Alfa Aesar, 99.7%), dimethyl sulfoxide-d_6 (Sigma-Aldrich, 99.9%), and deuterium chloride solution (Sigma-Aldrich, 35 wt % in D_2O, ≥99%) were used without any further purification. *No uncommon hazards are noted.*

The elemental distribution of the crystals was observed using a Hitachi TM3000 scanning electron microscope (SEM) equipped with a Bruker XFlash MIN SVE for energy-dispersive spectroscopy (EDS), operated at 15 kV. Fourier transform infrared (FTIR) spectroscopy measurements were performed on a Jasco 6100 FTIR instrument in attenuated total reflectance (ATR) mode (JASCO ATR PRO450-S). ^{1}H nuclear magnetic resonance (NMR) spectra were collected on a Magritek Spinsolve 60 MHz NMR spectrometer. Spectra were referenced to residual deuterated solvents and analyzed with Spinsolve software (v1.19.2). For analysis of MOFs by ^{1}H NMR spectroscopy, MOF powders were treated with 10 μL of deuterium chloride (35 wt % in D_2O), followed by the addition of 600 μL of dimethyl sulfoxide-d_6.

Synthesis of Azo@Ln-MOF (Ln = Ce, Pr, Nd). Ln-based MOFs were prepared based on a collective analysis of the literature procedures.[49,50] In a half-dram vial, adipic acid (3.7 mg, 25 μmol), 4,4′-azopyridine (4.6 mg, 25 μmol), and the corresponding lanthanide chloride (25 μmol) were dissolved in 150 μL of water and 19 μL of 28% ammonium hydroxide. The solution was then heated to 120 °C over 2 h, held at this temperature for 22 h, and then slowly cooled to room temperature over 2 h. Upon cooling to room temperature, pale-yellow crystals along with brown cocrystals of the organic linkers were observed (Figure S1).[51] The resulting pale-yellow crystals were solvent-exchanged with DMF (3 × 1 mL) to remove excess adipic acid and 4,4′-azopyridine (including cocrystals) before further characterization. In a separate experiment, the identity of the brown cocrystals was determined to be adipic acid and 4,4′-azopyridine via single-crystal X-ray diffraction (*vide infra*). The phase purity of the washed bulk MOFs was determined by powder X-ray diffraction (PXRD) before being subjected to further analysis (Figures 1 and S2).

Single-Crystal and Powder X-ray Diffraction. Single-crystal X-ray diffraction data were collected using a Rigaku XtaLAB Synergy-S X-ray diffractometer equipped with a Mo-target (λ = 0.71073 Å) and a HyPix-3000 hybrid pixel array detector, operating at 50 kV and 1 mA. To ensure completeness and desired redundancy, the

https://doi.org/10.1021/acs.inorgchem.4c01283
Inorg. Chem. 2024, 63, 12810−12817

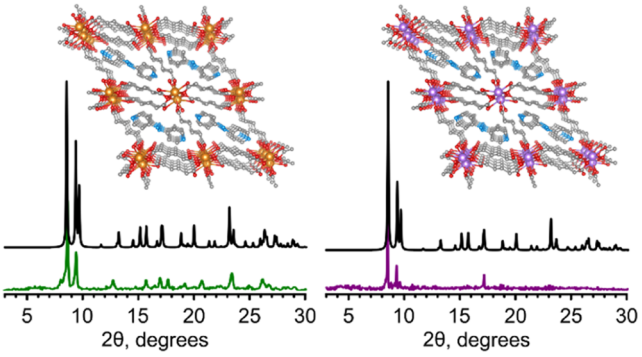

Figure 1. (*Left*) Single-crystal X-ray structure of Azo@Pr-MOF and associated simulated (black) and experimental (green) PXRD patterns. (*Right*) Single-crystal X-ray structure of Azo@Nd-MOF and associated simulated (black) and experimental (purple) PXRD patterns. The orange, purple, gray, red, and blue spheres represent praseodymium, neodymium, carbon, oxygen, and nitrogen atoms, respectively. Hydrogen atoms were omitted for clarity.

CrysAlisPro program was used for data collection strategy, data collection, and processing.[52] The structure was solved via intrinsic phase methods using ShelXT and refined using ShelXL in the Olex2 graphical user interface.[53−55] Further refinement details can be found in the Supporting Information. Crystallographic data can be found in Tables S1 and S2.

The phase purity of crystalline MOF powders was examined by room-temperature PXRD using a PANalytical X'Pert Pro MPD diffractometer with monochromatic Cu $K_{\alpha 1}$. Samples were loaded onto a zero-background plate (MTI Corporation) and collected at a scan rate of 1°/min with accelerating voltage and current of 45 kV and 40 mA, respectively.

Diffuse Reflectance Spectroscopy. Spectra were recorded on an Ocean Insight Ocean-HDX Miniature Spectrometer (OCEAN-HDX-UV−vis) connected to an Ocean Insight integrating sphere (ISP-REF) by using a 400 μm solarization-resistant SMA fiber optic cable (Ocean Insight, P400-2-SR). Time-resolved data was collected with an integration time of 6 ms at 10 scans to average and with a boxcar width of 5. The sample window of the integrating sphere was covered with a neutral density filter (Thorlabs, NE202B, optical density: 0.2) due to detector saturation by unfiltered light. Quartz plates (35 mm × 50 mm) with a sample well (Ø2 mm × 1 mm) were used for sample loading, and samples were referenced to a Spectralon total reflection standard (Labsphere, SRS-99-010). MOFs were irradiated by a mounted high-powered LED (Thorlabs M300L4) to induce the photoisomerization of azobenzene molecules. An LEDD1B (Thorlabs) power supply was used to power the LED at 350 mA. All samples were irradiated for 30 s at a distance of 1.0 cm. The power density at the surface of the powder under 300 nm irradiation was determined to be 1.91 mW/cm^2 using an optical power meter (Thorlabs, PM100D) equipped with a standard photodiode power sensor (Thorlabs, S120VC). The samples were measured at ambient temperatures. The photoisomerization rates were found for all samples by monitoring the attenuation at 492 nm over time under white light, after 300 nm irradiation, and fitting the decay with first-order rate kinetics.

RESULTS AND DISCUSSION

The choice of metal−organic platforms for the integration of stimuli-responsive fragments was based on several factors. In general, lanthanides, Ce(III), Pr(III), and Nd(III) were chosen for the framework synthesis due to their unique optical properties associated with a largely undisturbed 4*f*-electron shell that is shielded by occupied $5s^2$ and $5p^6$ orbitals.[8,11−14] Moreover, their pairing with appropriate organic ligands or chromophores could allow for the development of novel benchmark materials suitable for photodiode or luminometric dosimeter development.[1−3,5−10] The choice of the organic linker was dictated by its photophysical profile as well as the potential for preparation of frameworks possessing suitable pore sizes, allowing for integration of the selected stimuli-responsive moieties. Adipic acid coordination with lanthanide centers was previously employed for the preparation of frameworks possessing reasonable pores sizes for guest integration (e.g., 4,4′-bispyridine)[49,50] and was therefore selected as the nonphotochromic organic linker for MOF preparation. Next, 4,4′-azopyridine was selected as a compatible photochromic moiety to bestow control over the photophysical properties of adipic acid-based Ln-MOFs. Moreover, azobenzene undergoes *trans*- to *cis*-photoisomerization and can be influenced by ligand functionalities.[56−58] Notably, 4,4′-azopyridine has pyridyl functionalities capable of ligand−metal interactions and is relatively small in size (~9.0 Å along the molecular backbone) for noncoordinative immobilization within the MOFs' pores. Thus, the choice of selected building blocks was based on a combination of several factors including the MOF pore size and geometry considering previously reported frameworks[49,50] and ligand−metal interactions that can influence the photoswitches' photophysical response.[56−58]

Frameworks [Ce(adipate)][(4,4′-azopyridine)] (Azo@Ce-MOF, Scheme 1), [Pr(adipate)][(4,4′-azopyridine)] (Azo@Pr-MOF, Figure 1), and [Nd(adipate)][(4,4′-azopyridine)] (Azo@Nd-MOF, Figure 1) were prepared by heating the corresponding metal salt, adipic acid, and 4,4′-azopyridine under hydrothermal conditions in the presence of an ammonium hydroxide modulator (see the Experimental Section for details). Upon cooling of the reaction mixture, pale-yellow crystals were observed in all cases. The identity of the crystals was determined through single-crystal X-ray diffraction. The pale-yellow crystals were MOFs bearing the photochromic guest moiety (Azo@Ce-MOF, Azo@Pr-MOF, and Azo@Nd-MOF) as shown in Scheme 1 and Figure 1. After a solvent exchange procedure to remove excess organic linkers (*i.e.*, adipic acid or 4,4′-azopyridine), the resulting MOF single crystals were subjected to PXRD analysis to confirm the phase purity of the bulk material (Figures 1 and S2). As a next step, ^{1}H NMR spectroscopic analysis of the digested (destroyed in the presence of acid) Ln-MOF samples was used to determine the amount of 4,4′-azopyridine loading within the MOF pores. As an example, the ^{1}H NMR spectrum of the digested Azo@Pr-MOF can be found in Figure 2, which shows a mixture of 4,4′-azopyridine and adipic acid in a 0.88:1.00 ratio. Such a high loading of guest molecules allowed us to crystallographically resolve the integrated stimuli-responsive molecules (Scheme 1 and Figure 1). It is worth noting that upon excessive solvent exchanges with DMF (e.g., 10 × 1 mL), some 4,4′-azopyridine moieties can be extracted from the MOF pores (Figure S3). The ratio of installed linkers is then reduced to 0.30:1.00. Thus, all experiments were performed after 3 × 1 mL of solvent exchanges with DMF to retain photochromic functionality while still removing surface-bound impurities. In addition, FTIR spectroscopy was employed on MOF powders to support the integration of 4,4′-azopyridine within the framework. FTIR spectra of all 4,4′-azopyridine-containing MOFs (and 4,4′-azopyridine, neat) show coupled δ(C−H: in-plane bend) and ν(C−C: stretch) at 1322 cm^{-1} (Figure 2).[59] Further, the elemental distribution within the MOF crystals was analyzed by SEM-EDS. SEM-EDS maps of Azo@Ln-

https://doi.org/10.1021/acs.inorgchem.4c01283
Inorg. Chem. 2024, 63, 12810−12817

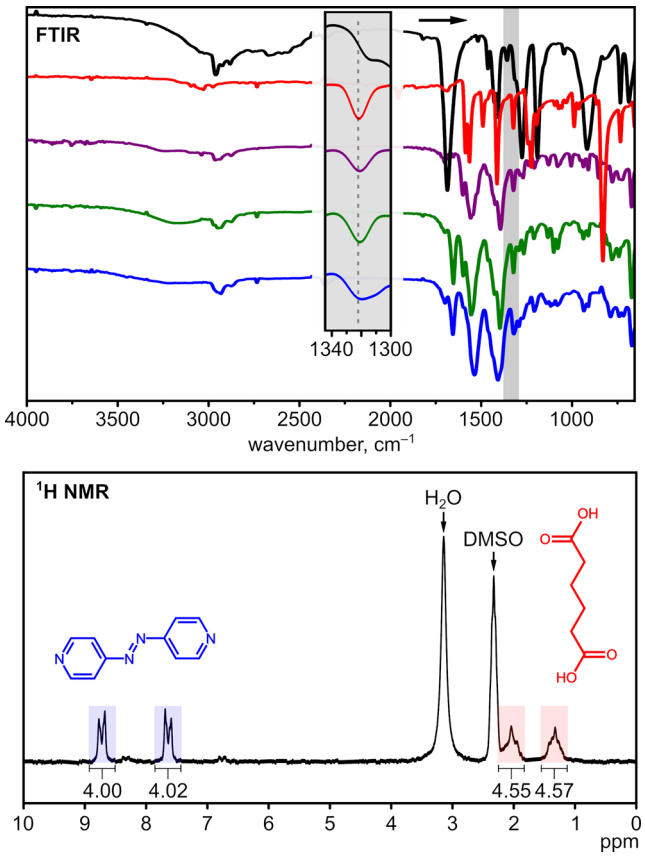

Figure 2. (*Top*) FTIR spectra of (blue) Azo@Ce-MOF, (green) Azo@Pr-MOF, (purple) Azo@Nd-MOF, (red) 4,4′-azopyridine, and (black) adipic acid. The inset shows δ(C−H: in-plane bend) coupled to ν(C−C: stretch) at 1322 cm^{-1} in 4,4′-azopyridine and MOFs containing 4,4′-azopyridine.[59] (*Bottom*) ^{1}H NMR spectrum of digested Azo@Pr-MOF in dimethyl sulfoxide-d_6. The resonances corresponding to 4,4′-azopyridine and adipic acid are colored blue and red, respectively.

MOFs (Figure S4) reveal an even distribution of C, N, O, and Ln (Ln = Ce, Pr, or Nd). The SEM images and EDS maps of Azo@Ce-MOF, Azo@Pr-MOF, and Azo@Nd-MOF can be found in the Supporting Information (Figures S5−S7).

An analysis of the single-crystal data shows that the three synthesized MOFs are isostructural, all crystallizing in the triclinic $P\bar{1}$ space group, with the asymmetric unit found to contain 1/2 of the trapped 4,4′-azopyridine. In the secondary building units (SBUs), a nine-coordinate lanthanide metal center is formally connected to a total of nine oxygen atoms from six adipic acid molecules (i.e., two bidentate, four monodentate relative to each specific metal center) and a coordinated water molecule. Such a coordination environment leads to a distorted tricapped trigonal antiprism geometry for each metal center (Figure S8). The SBUs are bridged by a series of adipate linkers bound in either a monodentate or bidentate fashion, with each metal center being connected to the next metal site via two chelating bridging modes (μ_2-η^2-η^1), and two bridging modes (μ_2-η^1-η^1). Throughout the lattice, there are solvent-accessible pores (~15 Å in diameter), where 4,4′-azopyridine is trapped via hydrogen-bonding interactions with the water molecules coordinated to the lanthanide-based metal nodes. In the absence of 4,4′-azopyridine, the coordinated water molecule forms a hydrogen-bonding interaction to chelate-bridging oxygen of the adipate, although in some cases both interactions are present. Selected bond lengths are highlighted in Table S3.

After suitable synthetic routes were established for the preparation of novel isostructural azobenzene-containing MOFs, the ability to tailor the optical profile of lanthanide-based materials via the incorporation of photochromic units was investigated. For this, the photophysical response of 4,4′-azopyridine (5 mM in ethyl acetate) was first evaluated using UV−vis spectroscopy in solution and used as a reference. Upon exposure of the 4,4′-azopyridine solution to a 300-nm excitation wavelength for 30 s, the absorbance band centered at 400 nm intensifies, which is in line with the previous literature reports of azobenzene derivatives in organic solvents and corresponds to *trans*- to *cis*-photoisomerization.[60] Subsequent exposure of the solution to visible light resulted in attenuation of the absorbance feature at 400 nm, indicating the expected *cis*- to *trans*-photoisomerization.[60] Analysis of absorbance attenuation at 400 nm as a function of time and fitting the data as a first-order exponential decay allowed us to determine the rate constant for the *cis*- to *trans*-photoisomerization of 4,4′-azopyridine in solution (5 mM ethyl acetate). Indeed, the rate constant was determined to be $k = 8.2 \times 10^{-3}$ s^{-1} (R^2 = 0.98, Figure S9).

As the next step, diffuse reflectance studies were performed on 4,4′-azopyridine-containing MOFs in the solid state. First, the diffuse reflectance profile for each MOF as-synthesized (i.e., without exposure to the mentioned 300-nm excitation wavelength) was collected as a reference point. The diffuse reflectance profiles of Nd- and Pr-containing MOFs contained several additional sharp signals that do not correlate with the photophysical response of embedded 4,4′-azopyridine (Figure 3) and appeared due to the presence of lanthanide ions.[61] For

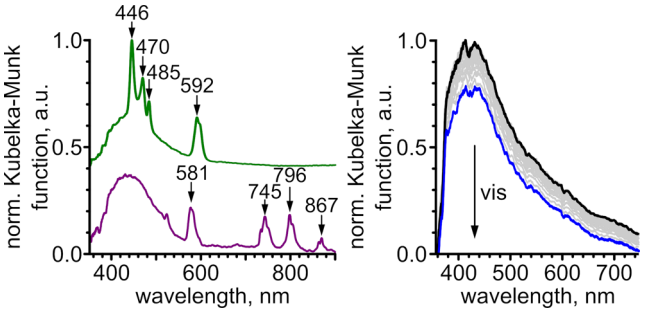

Figure 3. (*Left*) Normalized diffuse reflectance spectra of Azo@Pr-MOF (green) and Azo@Nd-MOF (purple). The wavelengths of the sharp absorption features in Pr- and Nd-containing samples are marked. (*Right*) Normalized diffuse reflectance spectra of Azo@Ce-MOF after 30 s of 300 nm irradiation (black) followed by attenuation under visible light (blue).

instance, in the case of Azo@Pr-MOF, there are four additional peaks in the diffuse reflectance profile at λ = 446, 470, 485, and 592 nm, while the diffuse reflectance profile of Azo@Nd-MOF contains four peaks at λ = 581, 745, 796, and 867 nm. These featured sharp absorption bands are characteristic of *f*-*f* transitions for the selected lanthanides and are in line with the previously reported ones for the lanthanide-based salts.[61] The Azo@Ce-MOF does not contain any additional sharp absorbance peaks beyond the broad absorption in the 350−550 nm range (Figure S10).

After the initial optical profiles of the prepared azobenzene-containing lanthanide-based MOFs were analyzed, the stimuli-

https://doi.org/10.1021/acs.inorgchem.4c01283
Inorg. Chem. 2024, 63, 12810−12817

responsive behavior of 4,4′-azopyridine integrated in the porous scaffolds was evaluated. Similar to the photophysical measurements of 4,4′-azopyridine in solution, each of the MOF samples with integrated photoresponsive 4,4′-azopyridine was exposed to a 300 nm excitation wavelength for 30 s, which resulted in a broad absorption feature in the 350−550 nm range for all presented MOFs as shown in Figure 3. Next, exposure to visible light resulted in attenuation of the absorption feature from 350 to 550 nm, which coincides with the behavior detected for 4,4′-azopyridine in solution. The attenuation of the absorbance at 492 nm upon exposure to visible light was fit as a first-order exponential decay, and the rate constants for the MOF samples were determined as $k = 2.8 \times 10^{-2}$, 3.5×10^{-2}, and 1.5×10^{-2} s^{-1}, for Azo@Ce-MOF, Azo@Pr-MOF, and Azo@Nd-MOF, respectively (Figures 3 and S11−S13). Thus, we found that the *cis*- to *trans*-photoisomerization of 4,4′-azopyridine within the MOFs' pores occurs even more rapidly than in solution, which is in line with several previous observations.[16,62−66] In addition to these experiments, we performed optical cycling experiments on Azo@Pr-MOF to confirm the repeatability of the photoisomerization process using alternating 300 nm and white-light irradiation (Figure S14).

Based on the enhanced photoisomerization kinetics (approximately 4.3-fold faster in Azo@Pr-MOF compared to solution) of 4,4′-azopyridine embedded in the prepared lanthanide-based MOFs in comparison with that of the same compound in solution, it is reasonable to anticipate that the lanthanide-MOF pore environment impacts the photoisomerization pathway. The exact mechanism for the photoisomerization of azobenzene and its derivatives is still under discussion in the literature and is hypothesized to proceed through either a rotational or an inversion transition state.[31,67−71] Depending on the transition state, for example, adding push−pull electronics to the azobenzene molecule through substitution or coordination (e.g., a dimethylamino group at the C4 (i.e., para) position and a nitro group at the C4′ position of azobenzene),[56,57] could alter the relaxation time. The *cis*- to *trans*-relaxation time could be also altered by replacing a phenyl ring of azobenzene with a pyridinium ring that has more powerful electron-withdrawing functionality than the NO_2 group as shown on the example of the polymeric systems.[41] As such, we envision that the noncoordinative integration of azobenzene derivatives within this MOF platform probably influences the relaxation mechanism.[31,67−71] A follow-up report on the electronic structure of azobenzene-embedded lanthanide-based MOFs and their effect on electronic transition states and push−pull mechanics is underway.

CONCLUSIONS

Driven by growing interest in a new generation of diode materials, optical and magnetic sensors, or ratiometric thermometers, these studies showcase the almost untapped potential of lanthanide-organic materials to promote cooperativity between photochromic molecules and lanthanide metal centers on the example of three novel photochromic 4,4′-azopyridine-based Ln-MOFs. A comprehensive analysis demonstrating the possibility of tailoring material properties through the employment of photochromic moieties includes single-crystal X-ray diffraction studies of the presented isostructural series of Ln-MOFs that shed light on the coordination environment of lanthanide cations in the prepared extended structures. Furthermore, the photophysical response of synthesized metal−organic materials was tailored on demand through the integration of photoresponsive 4,4′-azopyridine within the rigid matrix of Ln-based frameworks. At the same time, time-resolved spectroscopic analysis demonstrated that not only do noncoordinatively integrated photochromic moieties affect material properties but also the metal−organic matrix affects the photophysics of 4,4′-azopyridine units as well. Furthermore, the photoisomerization kinetics of a photochromic azobenzene derivative integrated within Ce-, Nd-, and Pr-based MOFs were determined for the first time, which demonstrated enhancement of rates for the photochromic 4,4′-azopyridine unit upon its integration within the rigid matrix compared to that in solution. Thus, the material properties are significantly tailored through the integration of a stimuli-responsive unit, as well as the optical properties of a photochromic unit that can be affected by a rigid lanthanide-containing host. Thus, the described cooperativity between the photophysics of photoresponsive guests and optically active lanthanide-based frameworks creates a possible pathway to tailor the optical properties of the material but also gain fundamental insights on the photophysics tunability of stimuli-responsive moieties integrated within a rigid multifaceted platform such as lanthanide-based organic frameworks.

ASSOCIATED CONTENT

Supporting Information

The Supporting Information is available free of charge at https://pubs.acs.org/doi/10.1021/acs.inorgchem.4c01283.

Additional experimental details; X-ray structure refinement; PXRD patterns; SEM images; EDS maps; and FTIR, NMR, and diffuse reflectance spectra (PDF)

Accession Codes

CCDC 2342127−2342129 and 2342145 contain the supplementary crystallographic data for this paper. These data can be obtained free of charge via www.ccdc.cam.ac.uk/data_request/cif, by emailing data_request@ccdc.cam.ac.uk, or by contacting The Cambridge Crystallographic Data Centre, 12 Union Road, Cambridge CB2 1EZ, U.K.; fax: +44 1223 336033.

AUTHOR INFORMATION

Corresponding Author

Corey R. Martin − *Savannah River National Laboratory, Aiken, South Carolina 29808, United States;* orcid.org/0000-0003-4124-3618; Email: corey.martin@srnl.doe.gov

Authors

Grace C. Thaggard − *Department of Chemistry and Biochemistry, University of South Carolina, Columbia, South Carolina 29208, United States*

Ingrid Lehman-Andino − *Savannah River National Laboratory, Aiken, South Carolina 29808, United States*

Eduardo Mollinedo − *Savannah River National Laboratory, Aiken, South Carolina 29808, United States*

Binod K. Rai − *Savannah River National Laboratory, Aiken, South Carolina 29808, United States*

Matthew A. Page − *Savannah River National Laboratory, Aiken, South Carolina 29808, United States*

Kathryn Taylor-Pashow − *Savannah River National Laboratory, Aiken, South Carolina 29808, United States;* orcid.org/0000-0002-1986-0866

https://doi.org/10.1021/acs.inorgchem.4c01283
Inorg. Chem. 2024, 63, 12810−12817

Natalia B. Shustova − *Department of Chemistry and Biochemistry, University of South Carolina, Columbia, South Carolina 29208, United States;* orcid.org/0000-0003-3952-1949

Complete contact information is available at: https://pubs.acs.org/10.1021/acs.inorgchem.4c01283

Author Contributions

The manuscript was written through contributions of all authors. All authors have given approval to the final version of the manuscript.

Notes

The authors declare no competing financial interest.

■ ACKNOWLEDGMENTS

This work was supported by the Laboratory Directed Research and Development (LDRD) program within the Savannah River National Laboratory (SRNL). Research conducted at the SRNL was supported by Battelle Savannah River Alliance, LLC under Contract No. 89303321CEM000080 with the U.S. Department of Energy. The publisher acknowledges the U.S. Government license to provide public access under the DOE Public Access Plan (http://energy.gov/downloads/doe-public-access-plan). N.B.S. is grateful for support from the NSF Award (DMR-2103722). G.C.T. was supported by the National Science Foundation Graduate Research Fellowship under Grant No. DGE-2034711.

■ ABBREVIATIONS

MOF	metal−organic framework
SEM	scanning electron microscopy
EDS	energy-dispersive spectroscopy
FTIR	Fourier transform infrared
ATR	attenuated total reflectance
NMR	nuclear magnetic resonance
DMF	*N*,*N*-dimethylformamide
PXRD	powder X-ray diffraction
SBU	secondary building unit

■ REFERENCES

(1) Islamoglu, T.; Ray, D.; Li, P.; Majewski, M. B.; Akpinar, I.; Zhang, X.; Cramer, C. J.; Gagliardi, L.; Farha, O. K. From Transition Metals to Lanthanides to Actinides: Metal-Mediated Tuning of Electronic Properties of Isostructural Metal-Organic Frameworks. *Inorg. Chem.* **2018**, *57*, 13246−13251.

(2) Karmakar, A.; Li, J. Luminescent MOFs (LMOFs): recent advancement towards a greener WLED technology. *Chem. Commun.* **2022**, *58*, 10768−10788.

(3) Wang, X.; Zhang, X.; Li, P.; Otake, K. I.; Cui, Y.; Lyu, J.; Krzyaniak, M. D.; Zhang, Y.; Li, Z.; Liu, J.; Buru, C. T.; Islamoglu, T.; Wasielewski, M. R.; Li, Z.; Farha, O. K. Vanadium Catalyst on Isostructural Transition Metal, Lanthanide, and Actinide Based Metal-Organic Frameworks for Alcohol Oxidation. *J. Am. Chem. Soc.* **2019**, *141*, 8306−8314.

(4) Reineke, T. M.; Eddaoudi, M.; Fehr, M.; Kelley, D.; Yaghi, O. M. From Condensed Lanthanide Coordination Solids to Microporous Frameworks Having Accessible Metal Sites. *J. Am. Chem. Soc.* **1999**, *121*, 1651−1657.

(5) Zhao, X.-Q.; Liu, X.-H.; Li, J.-J.; Zhao, B. Synthesis, structures, photoluminescence and magnetic properties of four-connected lanthanide-tricarboxylate coordination polymers. *CrystEngComm* **2013**, *15*, 3308−3317.

(6) Liang, Z.; Wu, H.; Singh, V.; Qiao, Y.; Li, M.; Ma, P.; Niu, J.; Wang, J. Assembly of Lanthanide-Containing Polyoxotantalate Clusters with Efficient Photoluminescence Properties. *Inorg. Chem.* **2019**, *58*, 13030−13036.

(7) Pagis, C.; Ferbinteanu, M.; Rothenberg, G.; Tanase, S. Lanthanide-Based Metal Organic Frameworks: Synthetic Strategies and Catalytic Applications. *ACS Catal.* **2016**, *6*, 6063−6072.

(8) Echenique-Errandonea, E.; Mendes, R. F.; Figueira, F.; Choquesillo-Lazarte, D.; Beobide, G.; Cepeda, J.; Ananias, D.; Rodríguez-Diéguez, A.; Paz, F. A. A.; Seco, J. M. Multifunctional Lanthanide-Based Metal-Organic Frameworks Derived from 3-Amino-4-hydroxybenzoate: Single-Molecule Magnet Behavior, Luminescent Properties for Thermometry, and CO2 adsorptive capacity. *Inorg. Chem.* **2022**, *61*, 12977−12990.

(9) Runowski, M.; Marcinkowski, D.; Soler-Carracedo, K.; Gorczyński, A.; Ewert, E.; Woźny, P.; Martín, I. R. Noncentrosymmetric Lanthanide-Based MOF Materials Exhibiting Strong SHG Activity and NIR Luminescence of Er3+: Application in Nonlinear Optical Thermometry. *ACS Appl. Mater. Interfaces* **2023**, *15*, 3244−3252.

(10) Errulat, D.; Marin, R.; Gálico, D. A.; Harriman, K. L. M.; Pialat, A.; Gabidullin, B.; Iikawa, F.; Couto, O. D. D., Jr; Moilanen, J. O.; Hemmer, E.; Sigoli, F. A.; Murugesu, M. A Luminescent Thermometer Exhibiting Slow Relaxation of the Magnetization: Toward Self-Monitored Building Blocks for Next-Generation Optomagnetic Devices. *ACS Cent. Sci.* **2019**, *5*, 1187−1198.

(11) Roy, S.; Chakraborty, A.; Maji, T. K. Lanthanide-organic frameworks for gas storage and as magneto-luminescent materials. *Coord. Chem. Rev.* **2014**, *273-274*, 139−164.

(12) Black, C. A.; Costa, J. S.; Fu, W. T.; Massera, C.; Roubeau, O.; Teat, S. J.; Aromí, G.; Gamez, P.; Reedijk, J. 3-D Lanthanide Metal-Organic Frameworks: Structure, Photoluminescence, and Magnetism. *Inorg. Chem.* **2009**, *48*, 1062−1068.

(13) Bünzli, J.-C.; Eliseeva, S. V. Intriguing aspects of lanthanide luminescence. *Chem. Sci.* **2013**, *4*, 1939−1949.

(14) Fang, Y.; Xing, C.; Zhan, S.; Zhao, M.; Li, M.; Liu, H.; Wang, C. Multifunctional Magnetic-Fluorescent Nanoparticle: Fabrication, Bioimaging, and Potential Antibacterial Applications. *ACS Biomater. Sci. Eng.* **2019**, *5*, 6779−6793.

(15) Jankowski, R.; Wyczasany, M.; Chorazy, S. Multifunctionality of luminescent molecular nanomagnets based on lanthanide complexes. *Chem. Commun.* **2023**, *59*, 5961−5986.

(16) Thaggard, G. C.; Maldeni; Kankanamalage, B. K. P.; Park, K. C.; Haimerl, J.; Fischer, R. A.; Shustova, N. B. Switching in Harmony: Tailoring the Properties of Functional Materials with Orthogonal Stimuli. *Chem. Phys. Rev.* **2024**, *5*, No. 011305.

(17) Mehlana, G.; Bourne, S. A. Unravelling chromism in metal-organic frameworks. *CrystEngComm* **2017**, *19*, 4238−4259.

(18) Rice, A. M.; Martin, C. R.; Galitskiy, V. A.; Berseneva, A. A.; Leith, G. A.; Shustova, N. B. Photophysics Modulation in Photoswitchable Metal-Organic Frameworks. *Chem. Rev.* **2020**, *120*, 8790−8813.

(19) Bandara, H. M. D.; Burdette, S. C. Photoisomerization in different classes of azobenzene. *Chem. Soc. Rev.* **2012**, *41*, 1809−1825.

(20) Gonzalez, A.; Kengmana, E. S.; Fonseca, M. V.; Han, G. C. D. Solid-state photoswitching molecules: structural design for isomerization in condensed phase. *Mater. Today Adv.* **2020**, *6*, No. 100058.

(21) Shao, B.; Aprahamaian, I. Hydrazones as New Molecular Tools. *Chem.* **2020**, *6*, 2162−2173.

(22) Torres-Zúñiga, V.; Morales-Saavedra, O. G.; Rivera, E.; Castañeda-Guzmán, R.; Bañuelos, J. G.; Ortega-Martínez, R. Preparation and photophysical properties of monomeric liquid-crystalline azo-dyes embedded in bulk and film SiO_2-sonogel glasses. *J. Sol−Gel Sci. Technol.* **2010**, *56*, 7−18.

(23) Magennis, S. W.; Mackay, F. S.; Jones, A. C.; Tait, K. M.; Sadler, P. J. Two-Photon-Induced Photoisomerization of an Azo Dye. *Chem. Mater.* **2005**, *17*, 2059−2062.

(24) Kinbara, K.; Aida, T. Towards Intelligent Molecular Machines: Directed Motions of Biological and Artificial Molecules and Assemblies. *Chem. Rev.* **2005**, *105*, 1377−1400.

(25) Hugel, T.; Holland, N. B.; Cattani, A.; Moroder, L.; Seitz, M.; Gaub, H. E. Single-molecule optomechanical cycle. *Science* **2002**, *296*, 1103−1106.
(26) Ichimura, K. Photoalignment of Liquid-Crystal Systems. *Chem. Rev.* **2000**, *100*, 1847−1874.
(27) Haque, H. A.; Kakehi, S.; Hara, M.; Nagano, S.; Seki, T. High-Density Liquid-Crystalline Azobenzene Polymer Brush Attained by Surface-Initiated Ring-Opening Metathesis Polymerization. *Langmuir* **2013**, *29*, 7571−7575.
(28) Miniewicz, A.; Girones, J.; Karpinski, P.; Mossety-Laszczak, B.; Galina, H.; Dutkiewicz, M. Photochromic and nonlinear optical properties of azo-functionalized POSS nanoparticles dispersed in nematic liquid crystals. *J. Mater. Chem. C* **2014**, *2*, 432−440.
(29) Russew, M.-M.; Hecht, S. Photoswitches: From Molecules to Materials. *Adv. Mater.* **2010**, *22*, 3348−3360.
(30) Bléger, D.; Schwarz, J.; Brouwer, A. M.; Hecht, S. *o*-Fluoroazobenzenes as Readily Synthesized Photoswitches Offering Nearly Quantitative Two-Way Isomerization with Visible Light. *J. Am. Chem. Soc.* **2012**, *134*, 20597−20600.
(31) Ren, H.; Yang, P.; Winnik, F. M. Azopyridine: A smart photo- and chemo-responsive substituent for polymers and supramolecular assemblies. *Polym. Chem.* **2020**, *11*, 5955−5961.
(32) Crespi, S.; Simeth, N. A.; König, B. Heteroaryl azo dyes as molecular photoswitches. *Nat. Rev. Chem.* **2019**, *3*, 133−146.
(33) Modrow, A.; Zargarani, D.; Herges, R.; Stock, N. Introducing a photo-switchable azo-functionality inside Cr-MIL-101-NH_2 by covalent post-synthetic modification. *Dalt. Trans.* **2012**, *41*, 8690−8696.
(34) Hermann, A. D.; Schwartz, H. A.; Werker, M.; Schaniel, D.; Ruschewitz, U. Metal-Organic Frameworks as Hosts for Fluorinated Azobenzenes: A Path Towards Quantitative Photoswitching with Visible Light. *Chem. - Eur. J.* **2019**, *25*, 3606−3616.
(35) Hermann, D.; Emerich, H.; Lepski, R.; Schaniel, D.; Ruschewitz, U. Metal-Organic Frameworks as Hosts for Photochromic Guest Molecules. *Inorg. Chem.* **2013**, *52*, 2744−2749.
(36) Li, Z.; Wang, G.; Ye, Y.; Li, B.; Li, H.; Chen, B. Loading Photochromic Molecules into a Luminescent Metal-Organic Framework for Information Anticounterfeiting. *Angew. Chem., Int. Ed.* **2019**, *58*, 18025−18031.
(37) Fernández, B.; Oyarzabal, I.; Seco, J. M.; Sebastián, E. S.; Fairen-Jiménez, D.; Gómez-Ruiz, S.; Salinas-Castillo, A.; Calahorro, A. J.; Rodríguez-Diéguez, A. Luminescence and Magnetic Properties of Two Three-Dimensional Terbium and Dysprosium MOFs Based on Azobenzene-4,4′-Dicarboxylic Linker. *Polymers* **2016**, *8*, 39.
(38) Huo, R.; Wang, C.; Wang, M. Y.; Sun, M. Y.; Jiang, S.; Xing, Y. H.; Bai, F. Y. Preparation of Naphthalenediimide-Decorated Electron-Deficient Photochromic Lanthanide (III)-MOF and Paper Strip as Multifunctional Recognition and Ratiometric Luminescent Turn-On Sensors for Amines and Pesticides. *Inorg. Chem.* **2023**, *62*, 6661−6673.
(39) Li, H.-S.; Xing, S.-H.; Xiao, Y.; Wang, C.; Guan, Q.-L.; Bai, F.-Y.; Xing, Y.-H.; Xu, F. Stimulus-Responsive Lanthanide MOF Materials Encapsulated with Viologen Derivatives: Characterization, Photophysical Properties and Sensing on Nitrophenols. *Chem.—Eur. J.* **2023**, *29*, No. e202202810.
(40) Christina, L. C.; Gunlazuardi, J.; Zulys, A. Synthesis and characterization of lanthanide metal-organic framework with perylene 3,4,9,10-tetracarboxylate ligand. *IOP Conf. Ser.: Mater. Sci. Eng.* **2020**, *902*, No. 012046.
(41) Pang, Z. H.; Dang, L. L.; Yang, L. X.; Luo, F. Azo-MOFs showing controllable framework flexibility and consequently fine-tuned photomechanical crystal motion. *J. Solid State Chem.* **2019**, *277*, 182−186.
(42) Alzard, R. H.; Siddig, L. A.; Saleh, N.; Nguyen, H. L.; Nguyen, Q. A. T.; Ho, T. H.; Bui, V. Q.; Sethupathi, K.; Sreejith, P. K.; Alzamly, A. A new mode of luminescence in lanthanide oxalates metal-organic frameworks. *Sci. Rep.* **2022**, *12*, No. 18812.
(43) Martin, C. R.; Kittikhunnatham, P.; Leith, G. A.; Berseneva, A. A.; Park, K. C.; Greytak, A. B.; Shustova, N. B. Let the light be a guide: Chromophore communication in metal-organic frameworks. *Nano Res.* **2021**, *14*, 338−354.
(44) Park, J.; Sun, L.-B.; Chen, Y.-P.; Perry, Z.; Zhou, H.-C. Azobenzene-Functionalized Metal-Organic Polyhedra for the Optically Responsive Capture and Release of Guest Molecules. *Angew. Chem., Int. Ed.* **2014**, *53*, 5842−5846.
(45) Kume, S.; Kurihara, M.; Nishihara, H. Reversible *trans-cis* photoisomerization of azobenzene-attached bipyridineligands coordinated to cobalt using single UV light source and the Co(III)/Co(II) redox change. *Chem. Commun.* **2001**, 1656−1657.
(46) Torréns, M.; Ortiz, M.; Turner, A. P. F.; Beni, V.; O'Sullivan, C. K. Controlled Zn-Mediated Grafting of Thin Layers of Bipodal Diazonium Salt on Gold and Carbon Substrates. *Chem. − Eur. J.* **2015**, *21*, 671−681.
(47) Zhang, D.; Zhang, Y.; Gong, W.; Li, J.; Liu, S.; Ma, Y.; Zhao, Q. Manipulating Photoisomerization Rate of Triphenylethylene Derivative through Metal Coordination for Irradiation Time-Dependent Information Encryption. *Adv. Opt. Mater.* **2023**, *11*, No. 2300386.
(48) Moody, G.; Islam, M. S. Materials for ultra-efficient, high-speed optoelectronics. *MRS Bull.* **2022**, *47*, 475−484.
(49) de Lill, D. T.; Gunning, N. S.; Cahill, C. L. Toward Templated Metal-Organic Frameworks: Synthesis, Structures, Thermal Properties, and Luminescence of Three Novel Lanthanide-Adipate Frameworks. *Inorg. Chem.* **2005**, *44*, 258−266.
(50) de Lill, D. T.; Cahill, C. L. Synthesis and Characterization of a Praseodymium-Adipate Framework Templated with 1,2-bis(4-Pyridyl)ethane: Host-Guest Interactions and Structural Survey. *Cryst. Growth Des.* **2007**, *7*, 2390−2393.
(51) Zhang, J.; Wu, L.; Fan, Y. Heterosynthons in molecular complexes of azopyridine and 1,2-bis(4-pyridyl)ethylene with dicarboxylic acids. *J. Mol. Struct.* **2003**, *660*, 119.
(52) Oxford Diffraction. *CrysAlisPro Software System*; Rigaku Corporation: Oxford, UK, 2015.
(53) Sheldrick, G. M. SHELXT-Integrated space-group and crystal-structure determination. *Acta Crystallogr.* **2015**, *71*, 3−8.
(54) Sheldrick, G. M. Crystal structure refinement with SHELXL. *Acta Crystallogr.* **2015**, *C71*, 3−8.
(55) Dolomanov, O. V.; Bourhis, L. J.; Gildea, R. J.; Howard, J. A. K.; Puschmann, H. Olex2: a complete structure solution, refinement and analysis program. *J. Appl. Crystallogr.* **2009**, *42*, 339−341.
(56) Schultz, T.; Quenneville, J.; Levine, B.; Toniolo, A.; Martinez, T. J.; Lochbrunner, S.; Schmitt, M.; Shaffer, J. P.; Zgierski, M. Z.; Stolow, A. Mechanism and Dynamics of Azobenzene Photoisomerization. *J. Am. Chem. Soc.* **2003**, *125*, 8098−8099.
(57) García-Amorós, J.; Velasco, D. Recent advances towards azobenzene-based light-driven real-time information-transmitting materials. *Beilstein J. Org. Chem.* **2012**, *8*, 1003−1017.
(58) Goulet-Hanssens, A.; Barrett, C. J. Photo-control of biological systems with azobenzene polymers. *J. Polym. Sci., Part A: Polym. Chem.* **2013**, *51*, 3058−3070.
(59) Zhuang, Z.; Cheng, J.; Wang, X.; Yin, Y.; Chen, G.; Zhao, B.; Zhang, H.; Zhang, G. Spectroscopy of 4,4′-azopyridine by density functional theory and surface-enhanced Raman scattering. *J. Mol. Struct.* **2006**, *794*, 77−82.
(60) Poutanen, M.; Ikkala, O.; Priimagi, A. Structurally Controlled Dynamics in Azobenzene-Based Supramolecular Self-Assemblies in Solid State. *Macromolecules* **2016**, *49*, 4095−4101.
(61) Lambert, H.; Claux, B.; Sharrad, C.; Soucek, P.; Malmbeck, R. Spectroscopic studies of neodymium(III) and praseodymium(III) compounds in molten chlorides. *Procedia Chem.* **2016**, *21*, 409−416.
(62) Thaggard, G. C.; Park, K. C.; Lim, J.; Maldeni Kankanamalage, B. K. P.; Haimerl, J.; Wilson, G. R.; McBride, M. K.; Forrester, K. L.; Adelson, E. R.; Arnold, V. S.; Wetthasinghe, S. T.; Rassolov, V. A.; Smith, M. D.; Sosnin, D.; Aprahamian, I.; Karmaker, M.; Bag, S. K.; Thakur, A.; Zhang, M.; Tang, B. Z.; Castano, J. A.; Chaur, M. N.; Lerch, M. M.; Fischer, R. A.; Aizenberg, J.; Herges, R.; Lehn, J.-M.; Shustova, N. B. Breaking the photoswitch speed limit. *Nat. Commun.* **2023**, *14*, No. 7556.

https://doi.org/10.1021/acs.inorgchem.4c01283
Inorg. Chem. 2024, 63, 12810−12817

(63) Thaggard, G. C.; Haimerl, J.; Park, K. C.; Lim, J.; Fischer, R. A.; Maldeni Kankanamalage, B. K. P.; Yarbrough, B. J.; Wilson, G. R.; Shustova, N. B. Metal-Photoswitch Friendship: From Photochromic Complexes to Functional Materials. *J. Am. Chem. Soc.* **2022**, *144*, 23249−23263.
(64) Lyndon, R.; Konstas, K.; Ladewig, B. P.; Southon, P. D.; Kepert, C. J.; Hill, M. R. Dynamic Photo-Switching in Metal-Organic Frameworks as a Route to Low-Energy Carbon Dioxide Capture and Release. *Angew. Chem., Int. Ed.* **2013**, *52*, 3695−3698.
(65) Rice, A. M.; Martin, C. R.; Galitskiy, V. A.; Berseneva, A. A.; Leith, G. A.; Shustova, N. B. Photophysics Modulation in Photoswitchable Metal-Organic Frameworks. *Chem. Rev.* **2020**, *120*, 8790−8813.
(66) Williams, D. E.; Martin, C. R.; Dologopolova, E. A.; Swifton, A.; Godfrey, D. C.; Ejegbavwo, O. A.; Pellechia, P. J.; Smith, M. D.; Shustova, N. B. Flipping the Switch: Fast Photoisomerization in a Confined Environment. *J. Am. Chem. Soc.* **2018**, *140*, 7611−7622.
(67) Jerca, F. A.; Jerca, V. V.; Hoogenboom, R. Advances and opportunities in the exciting world of azobenzenes. *Nat. Rev. Chem.* **2022**, *6*, 51−69.
(68) Demchenko, A. P.; Tomin, V. I.; Chou, P.-T. Breaking the Kasha Rule for More Efficient Photochemistry. *Chem. Rev.* **2017**, *117*, 13353−13381.
(69) Nenov, A.; Borrego-Varillas, R.; Oriana, A.; Ganzer, L.; Segatta, F.; Conti, I.; Segarra-Marti, J.; Omachi, J.; Dapor, M.; Taioli, S.; Manzoni, C.; Mukamel, S.; Cerullo, G.; Garavelli, M. Uv-Light-Induced Vibrational Coherences: The Key to Understanding Kasha Rule Violation in *trans*-Azobenzene. *J. Phys. Chem. Lett.* **2018**, *9*, 1534−1541.
(70) Rau, H. Further evidence for rotation in the π,π^* and inversion in the n,π^* photoisomerization of azobenzenes. *J. Photochem.* **1984**, *26*, 221−225.
(71) Orstan, A.; Ross, J. B. A. Investigation of the β-cyclodextrin-indole inclusion complex by absorption and fluorescence spectroscopies. *J. Phys. Chem. A* **1987**, *91*, 5046−5050.

https://doi.org/10.1021/acs.inorgchem.4c01283
Inorg. Chem. 2024, 63, 12810−12817